RSC Advances

PAPER

View Article Online
View Journal | View Issue

Cite this: *RSC Adv.*, 2022, **12**, 31046

Understanding the role of 5d electrons in ferromagnetism and spin-based transport properties of $K_2W(Cl/Br)_6$ for spintronics and thermoelectric applications

Mukaddar Sk * and Saurabh Ghosh*

Received 21st March 2022
Accepted 2nd May 2022

DOI: 10.1039/d2ra01841a

rsc.li/rsc-advances

In this article, we have systematically investigated the structural, electronic, magnetic, and spin-based thermoelectric properties of $K_2W(Cl/Br)_6$ by first-principles calculation. The obtained negative formation energy confirmed the thermodynamic stability of $K_2W(Cl/Br)_6$, while the tolerance factor calculation showed their cubic phase stability. In addition, we have estimated the elastic constants which confirmed the mechanical stability of $K_2W(Cl/Br)_6$. Further, the spin-polarized band structure and density of states calculations revealed the half-metallic nature with high Curie temperature (T_c) values of 613 K and 597 K for K_2WCl_6 and K_2WBr_6, respectively. Moreover, we have studied the temperature variation of thermoelectric properties such as k_l, σ, k_e, S, PF, and ZT. Such results showed that higher ZT values for spin-down channels are obtained from ultra-low k_e, and high PF. Therefore, $K_2W(Cl/Br)_6$ are viable thermoelectric and spintronic materials.

1. Introduction

The advancement of spintronics and quantum computing technology has boosted the memory storage speed with multi-functional characteristics. This is a developing field which reduces magnetic chip size and enhances the memory speed by utilizing the electron spin and its charge.[1,2] The advanced spintronic technology also has novel achievements in non-volatile magnetic random-access memory.[3,4] These advancements can also be applied in electronic devices due to their low cost, faster data speed, and less power consumption.[5–7] In addition, the recent quantum technology takes advantage of electronic spin states in the digital display rather than the charge states of a typical electronic operation. The development of giant magnetic resistance (GMR) in 1998 boosted this technology,[8] where the electron spin can create an enormous difference in the resistance of alternative magnetic layers in the presence of external applied magnetic fields. Thus, the magnetic response of electronic charge and spin facilitate the low-powered, high-speed, non-volatile, and nano-size memory.[9,10]

The present scientific achievements of spintronics technology gave rise to the improvement of magneto-resistive random-access memory (MRAM), magnetic sensors, magnetic valves, read heads of magnetic hard drives, and giant magneto-resistive effect (GMR). Materials exhibiting the high spin polarization (SP) are suitable candidates for spintronics technology. Rather, for the half-metallic ferromagnetism (HMF) materials, one channel is metallic and the other one is insulating, which produces 100% SP, demonstrating that they are spintronics materials.[11,12] The first HMF was observed by de Groot *et al.* in Heusler alloy PtMnSb and NiMnSb in 1983.[13] After this, HMF was observed in many types of materials such as diluted magnetic semiconductors, perovskites, spinel chalcogenides, and double perovskites.[14,15] But, the major confront of spintronic materials are their phase instability at elevated temperature and clustering of magnetic ions greatly influences the functionality of spin. In later research, the phase instability issue was resolved at higher temperature, but the problem of clustering remains to be addressed. Nonetheless, a lot of transition-metal doped alloys were formed at room temperature, still the issue of clustering limits their applications.[16] To solve the problem of spin segregation, numerous procedures were adopted, where the doping of nonmagnetic elements into alloys is prominent. The FM behaviour has been reported in $Be_{1-x}C_xS$,[17] $Sn_{1-x}Mg_xO_2$,[18] *etc.* But these materials are expensive and have complicated production procurements.

Recently, Halide based double perovskites with chemical formula X_2YZ_6 (X = Cs, Rb, K Y = Os, Nb, Ta, W; Z = Cl, Br, I) have attracted considerable attention for spintronics applications due to their low cost, high Curie temperature (T_c), and good stability.[19–23] In X_2YZ_6, the d-orbital electrons of Y atom contributes significantly to the magnetic moment. Furthermore, it has been noted that the halide based double

Department of Physics and Nanotechnology, SRM Institute of Science and Technology, Kattankulathur, 603 203, Tamil Nadu, India. E-mail: mukaddarsk05@gmail.com; saurabhghosh2802@gmail.com

perovskites have ferromagnetism at high Curie temperature. However, there is a lack of detailed description on the physical properties of X_2YZ_6. In this article, we have taken $K_2W(Cl/Br)_6$ compounds to investigate their magnetic and spin-based transport properties by first-principles calculation. These $K_2W(Cl/Br)_6$ compounds have been prepared by Xu *et al.* and Epperson *et al.* from a stoichiometric mixture of K(Cl/Br) and $W(Cl/Br)_4$ and they have observed the cubic phase stability from the X-ray diffraction patterns.[24,25] However, existing literatures about these compounds are only limited to their structural studies. To the best of our knowledge, there is no detailed report available on magnetic and spin-based transport properties of $K_2W(Cl/Br)_6$. Our spin-polarized band structure and density of states calculations revealed the presence of half-metallic character in these materials with high Curie temperature. Thus, $K_2W(Cl/Br)_6$ compounds are emerging spintronics materials.

Besides spintronics applications, the lead-free halide based double perovskites have attracted considerable attention for photovoltaic and thermoelectric technology. A good photovoltaic material should have high optical absorption coefficient and conductivity, with low reflectivity. On the other hand, a material is efficient for thermoelectric technology, if it has high Seebeck coefficient (S), good electrical conductivity (σ), and low thermal conductivity (k).[26] Many lead-free halide based double perovskites are reported to have suitable photovoltaic and thermoelectric properties. For instance, Haq *et al.* predicted that Rb_2XGaBr_6 (X = Na, K) are promising photovoltaic and thermoelectric materials due to their optimum optical absorption coefficient and large ZT values, respectively.[52] Later, Iqbal *et al.* have shown the emerging photovoltaic and thermoelectric properties of Rb_2AlInX_6 (X = Cl, Br, I) due to their narrow band gap.[53] Also, Nawaz *et al.* reported that Rb_2YInX_6 (X = Cl, Br, I) are thermodynamically stable and they are suitable for photovoltaic and thermoelectric technology.[54] Instead of low thermal conductivity arising from the occupation of cations in the octahedral structure, it is very surprising that these halide based double perovskites are mainly studied for photovoltaic purposes. Only very few experimental studies were performed to investigate their thermoelectric properties and interestingly the research in the thermoelectric response is now growing.[27] In this article, we have carried out the spin-based thermoelectric properties of $K_2W(Cl/Br)_6$. We have computed the temperature variation of k_l, σ, k_e, S, PF, and ZT. The higher ZT values for spin-down channels have resulted from ultra-low k_e, and high PF. Thus, $K_2W(Cl/Br)_6$ are potential thermoelectric and spintronic materials.

2. Computational details

The electronic structure, magnetic properties and transport properties of $K_2W(Cl/Br)_6$ were investigated by using Wien2k[28] and BoltzTraP code.[29] We have employed PBEsol approximation to optimize the crystal structure in FM and AFM states.[30] However, PBEsol approximation underestimates the electronic bandgap on which magnetic and transport properties are dependent. Therefore, we have employed TB-mBJ formalism,[31] which can accurately predict the bandgap. In addition, due to the presence of heavy elements, SOC coupling is significant, that was added with TB-mBJ. The energy cut-off for geometry optimization was selected to be 520 eV. On the other hand, the average forces per ions were optimized to 0.002 eV $Å^{-1}$. Furthermore, we have considered a k mesh of $12 \times 12 \times 12$ for electronic calculation. The product of maximum wave vector and muffin tin radii is kept as $R_{MT} \times K_{max} = 8$, along with angular momentum vector $l = 10$ and Gaussian factor = 10. The level convergence is achieved to be 10^{-5} Ry self consistently by using the above-mentioned inputs. For transport properties calculation, we have considered a dense k-points of 150 000.

3. Results and discussion

3.1 Structural and mechanical stabilities

The halide based double perovskites $K_2W(Cl/Br)_6$ have a cubic phase with space group $Fm\bar{3}m$ (225).[32] The perspective view of $K_2W(Cl/Br)_6$ is shown in Fig. 1. The vacancies between the octahedra $W(Cl/Br)_6$ are occupied by K atoms whereas each octahedron is separated by the other octahedra through the 12-fold coordination system of (Cl/Br). In this structure, each K atom is surrounded by 12 (Cl/Br) atoms, whereas every W atom is coordinated with 6 (Cl/Br) atoms. Moreover, each $W(Cl/Br)_6$ is located at the corner and face center of the cubic system. The K, W, and (Cl/Br) atoms in the unit cells of both systems are positioned at (0.25, 0.25, 0.25) (0, 0, 0) and (x, 0, 0), respectively. The atomic positions in the structure are corrected by minimizing strain throughout the optimization process.

The optimized energy *versus* volume plot is shown in Fig. 2(a and b). It is noticeable from Fig. 2(a and b), that $K_2W(Cl/Br)_6$ compounds have positive energy difference between FM and AFM states indicates that the FM is more preferable because of more energy release in this process.

Curie temperature (T_c) of $K_2W(Cl/Br)_6$ are predicted through the Heisenberg classical model. e., $T_c = 2\Delta E/3xK_B$, where x is the contribution of W atom and ΔE is the energy difference between ferromagnetic and antiferromagnetic ground states, *i.e.* $\Delta E = E_{AFM} - E_{FM}$.[33,34] The computed T_c values are 613 K and 597 K for K_2WCl_6 and K_2WBr_6, respectively. The high T_c values make these compounds suitable for spintronic applications.

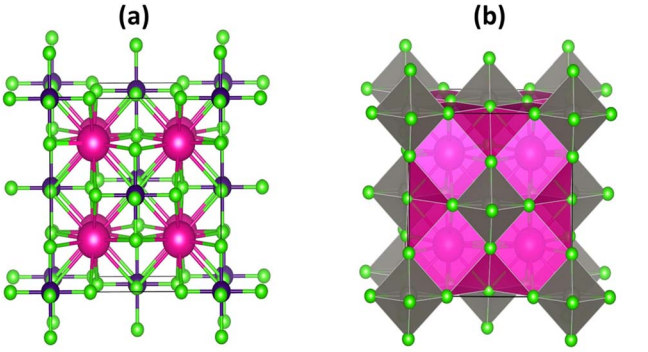

Fig. 1 The crystal structure (a) atomic and (b) polyhedral forms of $K_2W(Cl/Br)_6$ with magenta, blue and green colors represent the K, W, and (Cl/Br) atoms respectively.

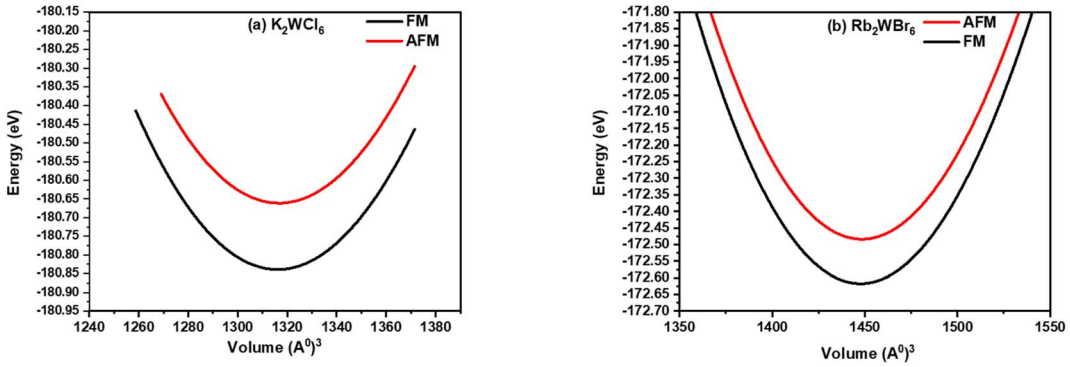

Fig. 2 Volume optimization plot of (a) K_2WCl_6 and (b) K_2WBr_6 in FM (black line) and AFM (red line) calculated through PBEsol approximation.

The cubic phase stability of $K_2W(Cl/Br)_6$ are investigated from Goldsmith tolerance fact or calculation as follows.

$$\tau = 0.707\frac{(R_A + R_X)}{(R_B + R_X)} \quad (1)$$

It is worthy to mention here that, the stable cubic phase should have τ value in the range of 0.9–1.02.[35] Table 1 clearly shows that τ values of $K_2W(Cl/Br)_6$ are in this range demonstrating their cubic phase stability.

To investigate the synthetic possibility of $K_2W(Cl/Br)_6$, we have calculated the enthalpy of formation by using the following equation

$$\Delta H_f = E_{total}\{K_2W(Cl/Br)_6)\} - 2E_K^{bulk} - E_W^{bulk} - 6E_{(Cl/Br)}^{bulk} \quad (2)$$

where, $E_{total}\{K_2W(Cl/Br)_6\}$, E_K^{bulk}, E_W^{bulk} and $E_{(Cl/Br)}^{bulk}$ represent the ground state energy of K_2WX_6, K, W, and (Cl/Br) in their bulk form. The predicted values of ΔH_f are −31.12 eV and −27.12 eV for K_2WCl_6 and K_2WBr_6, respectively. This negative ΔH_f revealed the thermodynamic stability of $K_2W(Cl/Br)_6$.

The mechanical stability was studied from elastic constant values (C_{ij}), obtained by using the Cubic Elastic package.[56] It is observed from Table 2 that the values of the various components of C_{ij} obeyed the Born criteria of mechanical stability, *i.e.* $C_{11} - C_{12} > 0$, $C_{44} > 0$, $C_{11} + 2C_{12} > 0$, $C_{12} < B < C_{11}$.[37] Furthermore, we have estimated the Cauchy's pressure (CP = C_{12}–C_{44}). The positive value of CP demonstrated the ductile properties of $K_2W(Cl/Br)_6$. The overall elastic study confirmed that $K_2W(Cl/Br)_6$ are mechanically stable.[36]

Table 1 The obtained lattice parameter (*a*), tolerance factor (τ), octahedral factor (μ), and formation energy (ΔH_f) of $K_2W(Cl/Br)_6$

Compound	a (Å)	τ	μ	ΔH_f (eV)
K_2WCl_6	10.71	0.98	0.45	−31.12
K_2WBr_6	10.75	0.98	0.44	−27.12

Table 2 The calculated bulk modulus (*B*), elastic constants (C_{ij}), and cauchy pressure (CP) of $K_2W(Cl/Br)_6$

Compound	*B* (GPa)	C_{11}	C_{12}	C_{44}	CP
K_2WCl_6	41.16	78.19	21.17	18.72	2.45
K_2WBr_6	39.33	74.89	20.76	18.41	2.35

3.2 Magnetic properties

The half-metallic ferromagnetic material having high spin polarization (*P*) is essential for spintronic applications. The spin polarization (*P*) can be obtained as

$$P = \frac{N_\uparrow(E_F) - N_\downarrow(E_F)}{N_\uparrow(E_F) + N_\downarrow(E_F)} \times 100 \quad (3)$$

where ($N_\uparrow$) and ($N_\downarrow$) represent the density of states of up and down the channels at Fermi level (E_F). The spin-polarized band structure is shown in Fig. 3. It is noticeable from Fig. 3 that, the quantum state of the spin-up channel overlapped with Fermi level (E_F), which demonstrates the metallic nature. However, the spin-down channel shows the insulating nature because of the existence of finite separation between valence band maxima (VBM) and conduction band minima (CBM). Therefore, the combined spin up and spin down showed the half-metallic ferromagnetism nature with 100% spin polarization ($P = 1$). The detailed investigation revealed that the valence band maxima (VBM) and conduction band minima (CBM) of spin-down channels are located at the same *k*-point for both compounds, which indicates the direct band gap properties. We have obtained the band gap of 3.01 eV and 2.72 eV for K_2WCl_6 and K_2WBr_6, respectively in the spin-down channel. Also, the estimated total magnetic moment is calculated to be $2\mu_B$ for both compounds. The integer value of total magnetic moment implies that $K_2W(Cl/Br)_6$ are half metallic ferromagnets. Thus, $K_2W(Cl/Br)_6$ are emerging spintronics materials.

For the detailed investigation of band structure results, we have further calculated the total and partial density of states of $K_2W(Cl/Br)_6$ as shown in Fig. 4(a–d). It is noticeable from Fig. 4(a and b) that the total DOS in the up spin showed the metallic behavior and the down spin presented the insulating behavior. Therefore, $K_2W(Cl/Br)_6$ are half-metallic ferromagnetism (HMF) in nature. To investigate the origin of half-metallic ferromagnetism (HMF) in $K_2W(Cl/Br)_6$, we have further investigated the partial density of states (PDOS) which is shown in

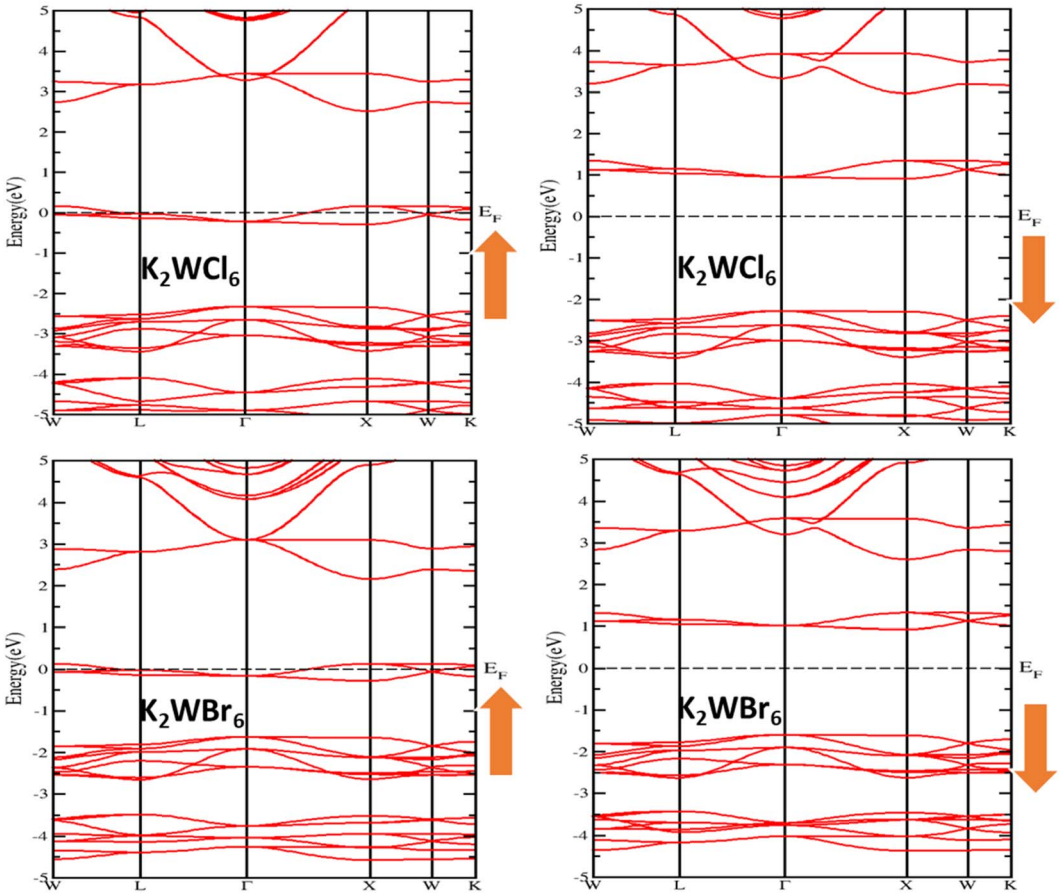

Fig. 3 The spin-polarized band structure of $K_2W(Cl/Br)_6$ calculated through mBJ + SOC.

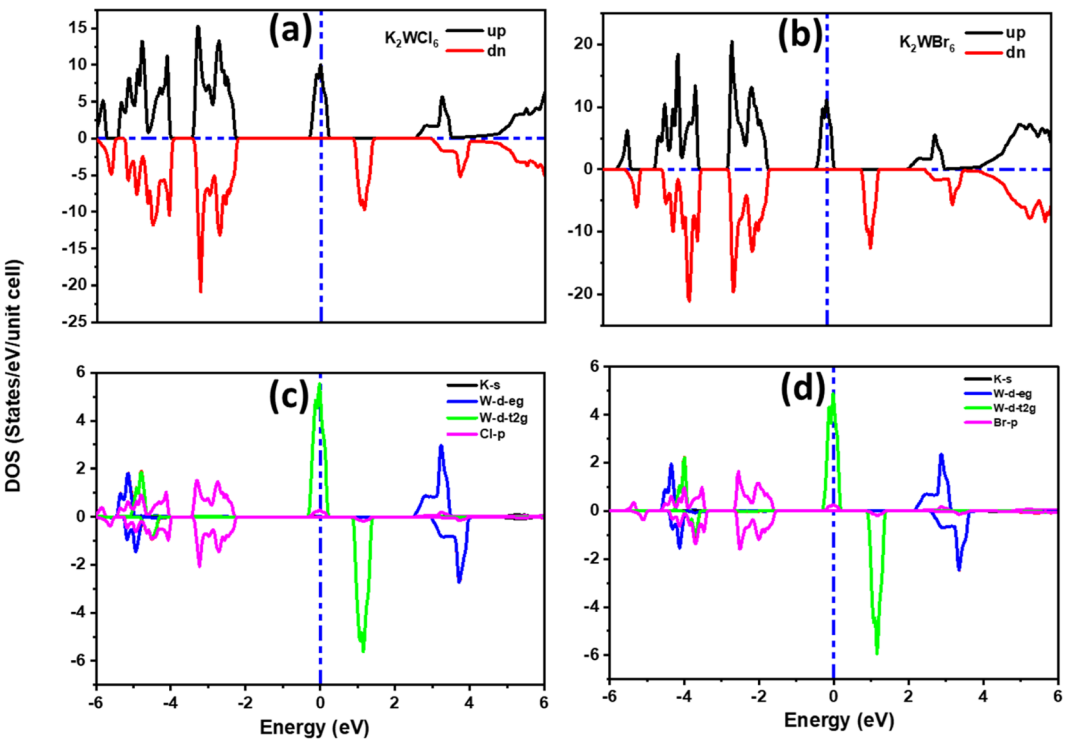

Fig. 4 The spin polarized (a and b) total DOS, (c and d) partial DOS of $K_2W(Cl/Br)_6$ obtained with mBJ + SOC.

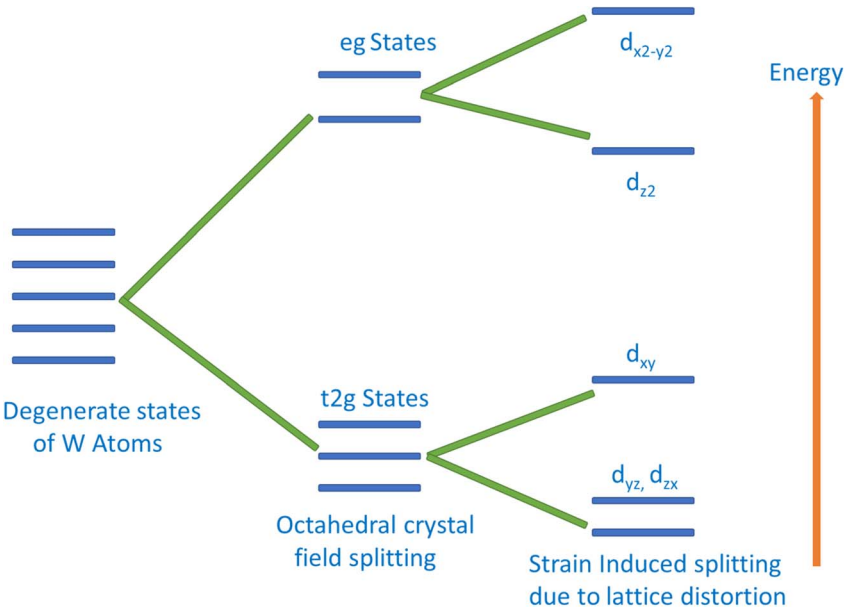

Fig. 5 Schematic representation of crystal-field splitting of W-5d orbital.

Fig. 4(c and d). It is evident from Fig. 4(c and d) that the d-t_{2g} states of W atoms are responsible for introducing HMF in $K_2W(Cl/Br)_6$. In the spin-up case, d-t_{2g} states of W atoms overlapped with Fermi level (E_F), which produces the metallic nature in $K_2W(Cl/Br)_6$. In the spin-down case, d-t_{2g} states move deep into the conduction band and thereby leaving a finite separation between the valence band and conduction band and therefore create insulating nature in $K_2W(Cl/Br)_6$.

The magnetic behavior of $K_2W(Cl/Br)_6$ has also been addressed by an exchange mechanism. The crystal field due to the Coulomb interaction between W and (Cl/Br) atoms split the 5d states of W into t_{2g} and e_g. The splitting of W-5d states is schematically shown in Fig. 5. It is clearly noticeable from Fig. 5 that the t_{2g} is triply degenerate (d_{xy}, d_{yz}, d_{zx}), which has lower energy than the double degenerate e_g (d_{z^2}, $d_{x^2-y^2}$) states. The splitting of e_g states results in the upward and downward shifting of $d_{x^2-y^2}$ and d_{z^2}, respectively. At the same time, splitting of t_{2g} state results in the increase of d_{xy} state energy and decrease of d_{yz} and d_{zx} states energies. The major magnetic response originated from the t_{2g} state of the W atom. This state is hybridized with the p state of (Cl/Br) *via* double exchange mechanism. Thus, we conclude that the double exchange mechanism between W atoms *via* (Cl/Br) atom is responsible for introducing HMF in $K_2W(Cl/Br)_6$.

3.3 Thermoelectric properties

Solid-state thermoelectric materials are gaining considerable attraction as novel materials for converting thermal to electrical energy.[38–42] Many mechanical and electronic devices release a huge amount of heat as waste. To take the advantage of wasted heat, efficient thermoelectric materials are needed which can directly convert the wasted heat into electricity. The thermoelectric performance of a material is given by a dimensionless parameter known as a figure of merit (ZT) given by; $ZT = \frac{S^2\sigma T}{(k_e + k_l)}$, where σ, S, T, k_e, and k_l represent the electrical conductivity, Seebeck coefficient, temperature, electrical thermal conductivity, and lattice thermal conductivity, respectively. The material with a large ZT value is considered to be a potential candidate for thermoelectric technology. But, obtaining a large ZT value is challenging due to the strong correlation of these physical properties. According to a recent report, magnetic interaction is one of the suitable approaches to enhance ZT.[43–47] The interaction of charge carriers with local magnetic moments, can enhance the carrier effective mass (m^*), consequently thermoelectric power ($S^2\sigma$) and corresponding figure of merit (ZT). It is worthy to mention here that such magnetic interaction is present in $K_2W(Cl/Br)_6$. Due to the

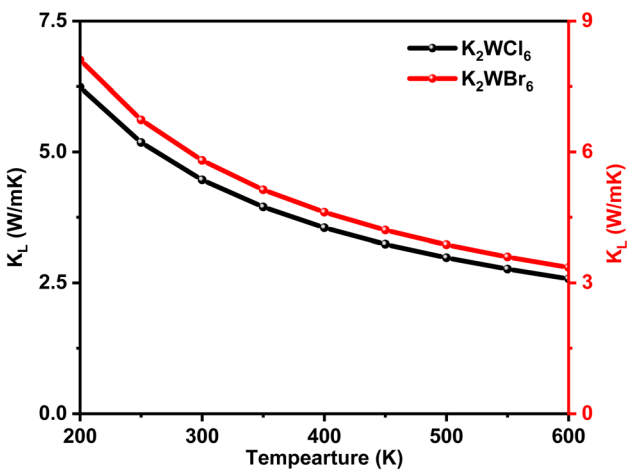

Fig. 6 The temperature-dependent lattice thermal conductivity (K_l) of $K_2W(Cl/Br)_6$ calculated through the Slack equation.

presence of magnetic interaction in $K_2W(Cl/Br)_6$, it is expected that these systems will have large ZT values. However, there are no detailed studies on thermoelectric properties of $K_2W(Cl/Br)_6$.

In this article, we have calculated the temperature variation of thermoelectric properties in $K_2W(Cl/Br)_6$. For this, we have employed BoltzTrap code.[24] During all calculations, the relaxation time (τ) is fixed by BoltzTraP code as $\tau = 10^{-14}$ s. We have separately calculated the thermoelectric parameters for spin-up and spindown configurations.

For thermoelectric calculation, the temperature was varied from 200 K to 600 K. The total thermal conductivity (k) is the sum of electronic (k_e) and lattice (k_l) thermal conductivities. A good thermoelectric material should have low k. The temperature variation of lattice thermal conductivity (k_l) was calculated by using the Slack equation.[55] The temperature variation of k_l is shown in Fig. 6. It can be seen from Fig. 6 that k_l has an inverse relationship with temperature, which is a typical feature of half-metallic ferromagnetic materials.[48] It is worthy to mention here that $K_2W(Cl/Br)_6$ compounds have low k_l values.

The amount of charge flow per unit time inside of a compound can be understood from its electrical conductivity (σ). The materials are categorized into insulator, semiconductor, and metal-based on their ability of charge flow.[49] A good thermoelectric material should have a large σ value.[50] The temperature variation of σ is calculated for $K_2W(Cl/Br)_6$ as shown in Fig. (a) and Fig. 8(a), respectively. The detailed analyses revealed that the σ value for spin-up configurations in $K_2W(Cl/Br)_6$ decreases with temperature until achieving the lowest value of $1.97 \times 10^5\ \Omega^{-1}\ m^{-1}$ (K_2WCl_6) and $2.25 \times 10^5\ \Omega^{-1}\ m^{-1}$ (K_2WBr_6) at 600 K. On the other hand, the values of σ for spin-up states in $K_2W(Cl/Br)_6$ are almost constant in the entire temperature up to 400 K. However, there was a gradual increase of σ is observed above 400 K. This trend of σ for up and down channels is typical feature in HMF.[51] The detailed investigation reveals that spin-up channel σ is dominant in both cases.

We have also examined the temperature variation of electronic thermal conductivity (k_e) as shown in Fig. 7(b) and 8(b) for K_2WCl_6 and K_2WBr_6, respectively. It is noticeable that k_e for spin-up configuration has a direct relation with temperature up to a certain limit where k_e increases to 3.41 W K^{-1} m^{-1} and 4.12 W K^{-1} m^{-1} respectively for K_2WCl_6 and K_2WBr_6, at 400 K. Above this temperature, k_e decreases gradually for both systems. On the other hand, the values k_e in spin-down states of $K_2W(Cl/Br)_6$ are 0.0 in the entire temperature up to 400 K. Above this temperature, k_e increases abruptly in both cases. It is worthy to mention here that k_e values for spin-down channels are very less compared to spin-up configuration.

The Seebeck coefficient (S) plays an important role to describe the thermoelectric performance. The S is defined by the ratio of a voltage difference to that of a temperature difference. It can also show the capability of a material to generate the thermo-electromotive force from a given temperature gradient. The S can be calculated by the following relation

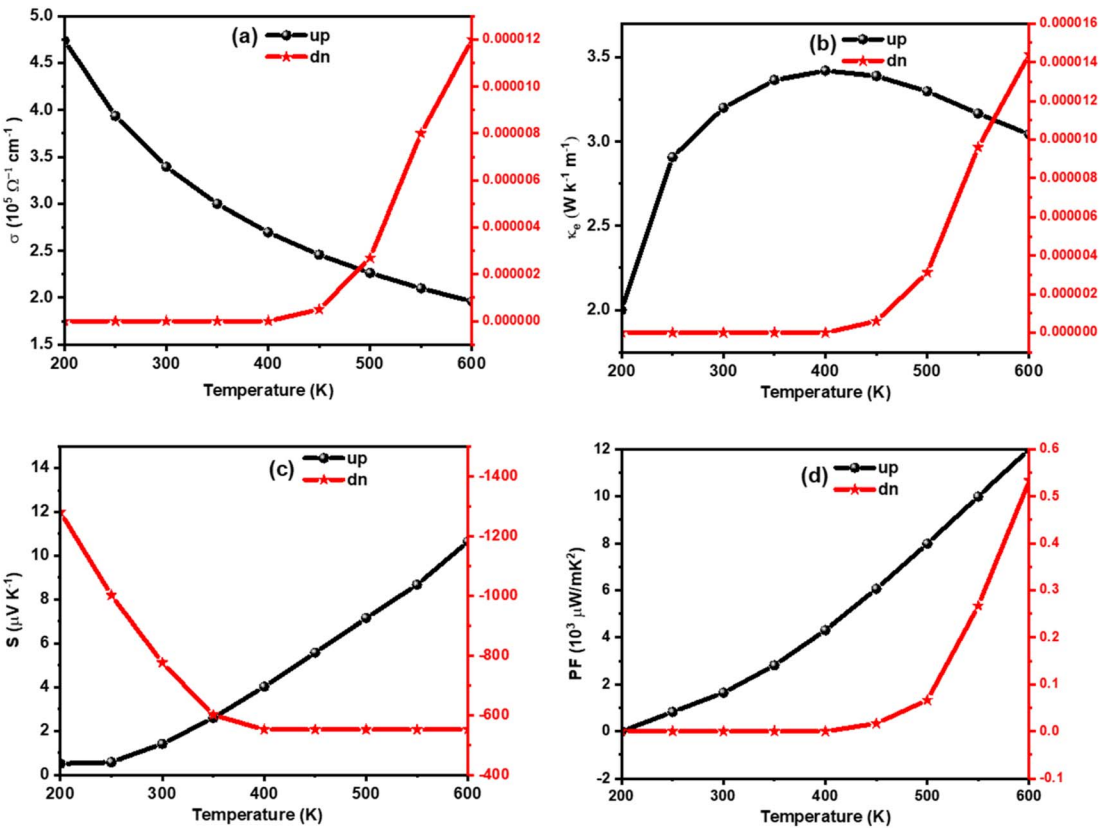

Fig. 7 Calculated (a) σ, (b) k, (c) S, and (d) PF of K_2WCl_6 as a function of temperature.

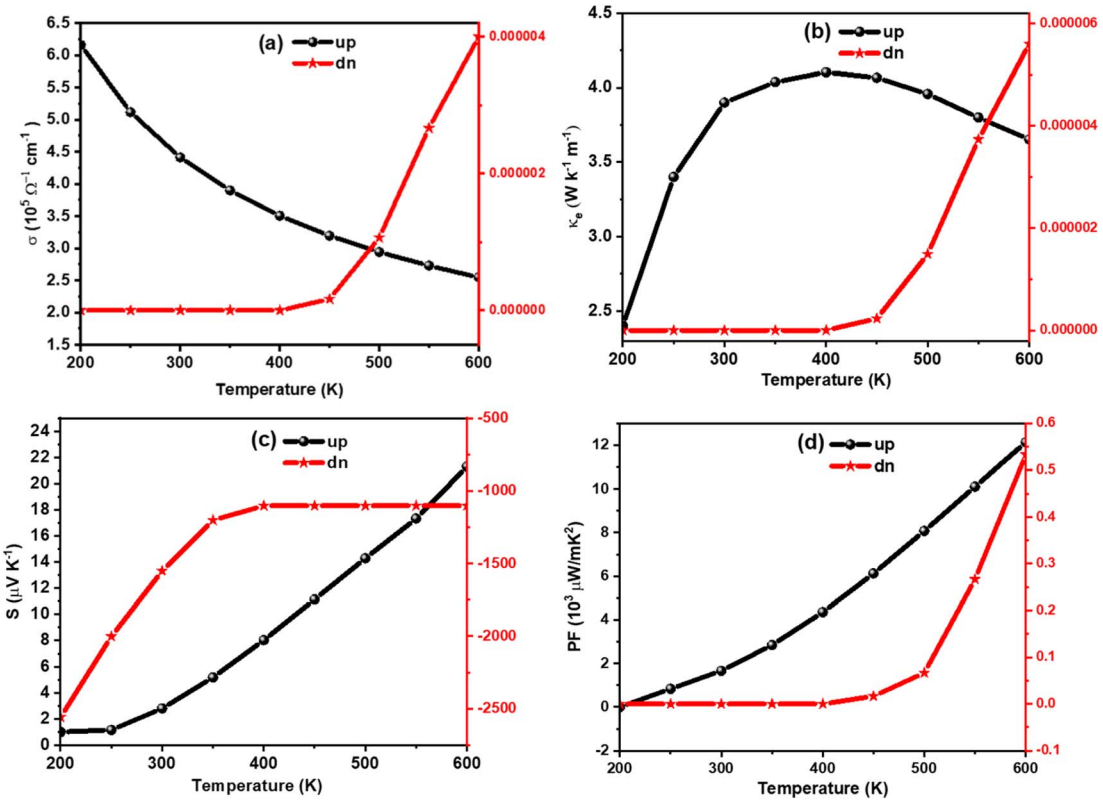

Fig. 8 Calculated (a) σ, (b) k, (c) S, and (d) PF of K_2WBr_6 as a function of temperature.

$$S(\uparrow,\downarrow) = \frac{8}{3e^2h}\pi^2 {k_B}^2 m^*(\uparrow,\downarrow)T\left(\frac{\pi}{3n}\right)^{\frac{2}{3}} \quad (4)$$

where h, k_B, e, m*(↑,↓), T, and n represent the Planck constant, Boltzmann constant, electronic charge, spin-dependent carrier effective mass, absolute temperature, and carrier concentration respectively. A good thermoelectric material should have a large Seebeck coefficient. Fig. 7(c) and 8(c) presented the Seebeck coefficients for both compounds in both spin configurations as a function of temperature. It is noticeable from Fig. 7(c) and Fig. 8(c) that the obtained values of Seebeck coefficients are positive in the entire temperature range of spin up channels, demonstrating the presence of p-type charge carriers (hole), whereas negative values Seebeck coefficients for a spin up channel suggest the presence n-type charge carriers (electron). The absolute value of S for spin up configuration in K_2WCl_6 (K_2WBr_6) increases from 0.67 μV K^{-1} (1.01 μV K^{-1}) at 200 K linearly up to 600 K. This increasing trend in up channel is due to its metallic nature. For metal, there is huge number of free electrons and hence applying a temperature gradient should lead to diffusion of more charge carriers towards cold end. As a result, the potential difference between two ends will increase

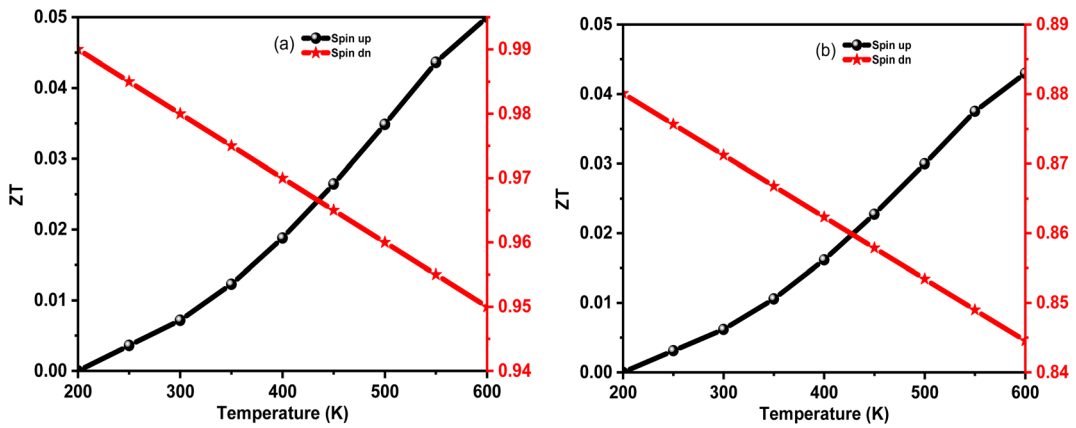

Fig. 9 The calculated ZT value of (a) K_2WCl_6 and (b) K_2WBr_6 as a function of temperature.

and therefore S will increase. In the spin-down channel, there is an abrupt decrease of S in K_2WCl_6 (K_2WBr_6) from a very high value of 1267 μV K^{-1} (1397 μV K^{-1}) at 200 K beyond this temperature S decreases gradually. This, decrease trend in spin-down channel can be described from eqn (4). The increasing of temperature can enhance the carrier concentration and thereby decreasing the value of S. The detailed investigation depicts that spin down channel Seebeck coefficient is dominant in both cases.

In addition, we have calculated the thermoelectric power factor (PF) as shown in Fig. 7(d) and Fig. 8(d). It is noticeable that the PF of spin-up configuration in K_2WCl_6 (K_2WBr_6) increases from 0.02×10^9 W mK^{-1} (0.01×10^9 W mK^{-1}) at 200 K linearly up to 600 K. On the other hand, the PF of spin-down state is found to be 0.0 μW mK^{-2} for both systems in the entire temperature up to 400 K. Beyond this temperature, the PF increases gradually.

Motivated by large S, σ, and PF with low k_e, we have calculated the temperature variation of thermoelectric figure of merit (ZT) as Fig. 9(a and b). The detailed analysis revealed that the ZT for spin upstate in K_2WCl_6 (K_2WBr_6) increases from 0.001 (0.001) at 200 K to 0.05 (0.041) at 600 K. On the other hand, ZT values of a spin-down channel in K_2WCl_6 (K_2WBr_6) gradually decrease from 0.99 (0.884) at 200 K to 0.95 (0.845) at 600 K. It is noticeable that spin down channel ZT value is dominant in both cases. The higher ZT value of the spin-down channel is due to its very low thermal conductivity. Also, the large ZT values demonstrated that $K_2W(Cl/Br)_6$ are potential thermoelectric materials.

4. Conclusion

To summarize this article, we have systematically investigated the structural, electronic, and thermoelectric properties of $K_2W(Cl/Br)_6$. The negative formation energy leads to the thermodynamic stability of $K_2W(Cl/Br)_6$. In addition, the spin-polarized band structure and density of states calculations revealed the presence of half-metallic character with higher T_c values, which are 613 K and 597 K for K_2WCl_6 and K_2WBr_6, respectively. Thus, $K_2W(Cl/Br)_6$ are potential candidates for spintronics application. Furthermore, the origin of half-metallic ferromagnetism is discussed with the double-exchange mechanism. Finally, we have computed the temperature variation of k_l,σ, k_e, S, PF, and ZT. The higher ZT values for spin-down channels have resulted from ultra-low k_e, and high PF. In short, $K_2W(Cl/Br)_6$ are potential thermoelectric and spintronic materials.

Data availability

The datasets produced for current study would be available from Mr Mukaddar Sk on reasonable request.

Conflicts of interest

The authors have no conflict of interest.

Acknowledgements

Mr Mukaddar Sk would like acknowledge CSIR-HRDG for fellowship grant 09/1045(0041)/2019-EMR-I.

References

1 T. Dietl, H. Ohno, F. Matsukura, J. Cibert and E. D. Ferrand, Zener model description of ferromagnetism in zinc-blende magnetic semiconductors, *Science*, 2000, **287**, 1019.
2 Y. Huai, F. Albert, P. Nguyen, M. Pakala and T. Valet, Observation of spin-transfer switching in deep submicron-sized and low-resistance magnetic tunnel junctions, *Appl. Phys. Lett.*, 2004, **84**, 3118.
3 C. Chappert C, A. Fert, F. Nguyen and V. Dau, The emergence of spin electronics in data storage, *Nat. Mater.*, 2007, **6**, 813.
4 M. C. Prestgard, G. P. Siegel and A. Tiwari, Oxides For Spintronics: A Review Of Engineered Materials For Spin Injection, *Adv. Mater. Lett.*, 2014, **5**, 242.
5 X. Li and J. Yang, First-principles design of spintronics materials, *Natl. Sci. Rev.*, 2016, **3**, 365.
6 S. Assefa, J. Nowak, J. Sun, E. O'Sullivan, S. Kanakasabapathy, W. Gallagher, Y. Nagamine, K. Tsunekawa, D. Djayaprawira and N. Watanabe, Fabrication, and characterization of MgO-based magnetic tunnel junctions for spin momentum transfer switching, *J. Appl. Phys.*, 2007, **102**, 063901.
7 K. L. Wang, J. G. Alzate and P. K. Amiri, Low-power non-volatile spintronic memory: STT-RAM and beyond, *J. Phys. D: Appl. Phys.*, 2013, **46**, 074003.
8 M. N. Baibich, J. M. Broto, A. Fert, F. N. van Dau, F. Petro, P. Eitenne, G. Creuzet, A. Friederich and J. Chazelas, Giant magnetoresistance of (001) Fe/(001)Cr magnetic superlattices, *Phys. Rev. Lett.*, 1988, **61**, 2472.
9 S. A. Wolf, D. D. Awschalom, R. A. Buhrman, J. M. Daughton, S. V. Molnár, M. L. Roukes, A. Y. Chtchelkanova and D. M. Treger, Spintronics: a spin-based electronics vision for the future, *Science*, 2001, **294**, 1488.
10 J. Puebla, J. Kim, K. Kondou and Y. Otani, Spintronic devices for energy-efficient data storage and energy harvesting, *Commun. Mater.*, 2020, **1**, 24.
11 W. E. Pickett and D. J. Singh, Electronic structure and half-metallic transport in the La_{1-x} Ca_xMnO_3 system, *Phys. Rev. B: Condens. Matter Mater. Phys.*, 1996, **53**, 1146.
12 D. J. Singh and W. Pickett, Pseudogaps Jahn–Teller distortions, and magnetic order in manganite perovskites, *Phys. Rev. B: Condens. Matter Mater. Phys.*, 1998, **57**, 88.
13 R. De Groot, F. Mueller, P. Van Engen and K. Buschow, New class of materials: half-metallic ferromagnets, *Phys. Rev. Lett.*, 1983, **50**, 2024.
14 Q. Lu, B. Wang, X. R. Chen and W. M. Liu, Robust large-gap quantum spin Hall insulators in methyl functionalized III-Bi buckled honeycombs, *Phys. Rev. Mater.*, 2018, **2**, 014005.
15 X. L. Zhang, L. F. Liu and W. M. Liu, Quantum anomalous Hall effect and tunable topological states in 3d transition metals doped silicene, *Sci. Rep.*, 2013, **3**, 2908.

16 T. Dietl, Origin and control of ferromagnetism in dilute magnetic semiconductors and oxides, *J. Appl. Phys.*, 2008, **103**, 07D111.
17 W. Akbar and S. Nazir, Origin of p-type half-metallic ferromagnetism in carbon-doped BeS: first-principles characterization, *J. Alloys Compd.*, 2018, **743**, 83.
18 C. W. Zhang and S. S. Yan, First-principles study on ferromagnetism in Mg-doped SnO_2, *Appl. Phys. Lett.*, 2009, **95**, 232108.
19 R. Ullah, M. A. Ali, G. Murtaza, A. Khan and A. Mahmood, *Ab initio* study for the structural, electronic, magnetic, optical, and thermoelectric properties of K_2OsX_6 (X Cl, Br) compounds, *Int. J. Energy Res.*, 2020, **44**, 9035.
20 M. A. Ali, G. Murtaza, A. Khan, E. Algrafy, A. Mahmood and S. M. Ramay, Magnetoelectronic properties of ferromagnetic compounds Rb_2TaZ_6 (Z Cl, Br) for possible spintronic applications, *Int. J. Quantum Chem.*, 2020, **120**, e26357.
21 M. Faizan, S. H. Khan, G. Murtaza, A. Khana and A. Laref, Electronic and magnetic properties of alkali metal chlorides A_2MCl_6 (A = K, Rb, Cs; M = Mn, Mo): A density functional theory study, *Int. J. Mod. Phys. B*, 2019, **33**, 1950072.
22 M. Faizan, S. H. Khan, A. Khan, A. Laref and G. Murtaza, *Ab-initio* prediction of structural, electronic and magnetic properties of Hexafluoromanganete(IV) complexes, *Int. J. Mod. Phys. B*, 2018, **32**, 1850270.
23 M. A. Ali, G. Murtaza and A. Laref, Exploring ferromagnetic half-metallic nature of Cs_2NpBr_6 *via* spin polarized density functional theory, *Chin. Phys. B*, 2020, **29**, 066102.
24 M. G. Brik and I. V. Kityk, Modeling of lattice constant and their relations with ionic radii and electronegativity of constituting ions of A2XY6 cubic crystals (A = K, Cs, Rb, Tl; X = tetravalent cation, Y = F, Cl, Br, I), *J. Phys. Chem. Solids*, 2011, **72**(11), 1256–1260, DOI: **10.1016/j.jpcs.2011.07.016**.
25 E. R. Epperson, *The Binary Halides Of Molybdenum(IV) And Tungsten(IV) and The Oxochlorides Of Tungsten(VI)*, 1965, **https://scholarlycommons.pacific.edu/cgi/viewcontent.cgi?article=3864&context=uop_etds**.
26 S. R. Bhandari, D. K. Yadav, B. P. Belbase, M. Zeeshan, B. Sadhukhan, D. P. Rai, R. K. Thapa, G. C. Kaphle and M. P. Ghimire, Electronic, magnetic, optical and thermoelectric properties of $Ca_2Cr_{1-x}Ni_xOsO_6$ double perovskites, *RSC Adv.*, 2020, **10**, 16179.
27 M. Nabi and D. C. Gupta, Potential lead-free small bandgap halide double perovskites Cs_2CuMCl_6 (M = Sb, Bi) green technology, *Sci. Rep.*, 2021, **11**, 12945.
28 P. Blaha, K. Schwarz, G. K. H. Madsen, D. Kvasnicka, and J. Luitz, *WIEN2k:An Augmented Plane Wave Plus Local Orbitals Program for Calculating Crystal Properties*, Vienna University of Technology, Austria, 2001, **https://www.researchgate.net/publication/237132866_WIEN2k_An_Augmented_Plane_Wave_plus_Local_Orbitals_Program_for_Calculating_Crystal_Properties**.
29 G. K. H. Madsen and D. J. Singh, BoltzTraP. A code for calculating band-structure-dependent quantities, *Comput. Phys. Commun.*, 2006, **175**, 67.
30 J. P. Perdew, K. Burke and M. Ernzerhof, Generalized Gradient Approximation Made Simple, *Phys. Rev. Lett.*, 1996, **77**, 3865.
31 F. Tran and P. Blaha, Accurate band gaps of semiconductors and insulators with a semilocal exchange-correlation potential, *Phys. Rev. Lett.*, 2009, **102**, 226401.
32 I. V. Fernandez, S. Mariotti, O. S. Hutter, M. Birkett, T. D. Veal, T. D. C. Hobson, L. J. Phillips, L. Danos, P. K. Nayak, H. J. Snaith, W. Xie, M. P. Sherburne, M. Asta and K. Durose, Vacancy-Ordered Double Perovskite Cs_2TeI_6 Thin Films for Optoelectronics, *Chem. Mater.*, 2020, **32**, 6676.
33 Q. Mahmood, M. Hassan and N. A. Noor, Systematic study of room temperature ferromagnetism and optical response of $Zn_{1-x}TM_xS/Se$ (TM Mn, Fe Co, Ni) ferromagnets: First principle approach, *J. Phys.: Condens. Matter*, 2016, **28**, 506001.
34 C. W. Zhang and S. S. Yan, First-principles prediction of half-metallic ferromagnetism in Cu-doped ZnS, *J. Appl. Phys.*, 2010, **107**, 043913, DOI: **10.1063/1.3309771**.
35 C. Li, X. Lu, W. Ding, L. Feng, Y. Gao and Z. Guo, Formability of ABX_3 (X = F, Cl, Br, I) halide perovskites, *Acta Crystallogr., Sect. B: Struct. Sci.*, 2008, **64**, 702.
36 M. Jamal, S. J. Asadabadi, I. Ahmad and H. A. R. Aliabad, Elastic constants of cubic crystals, *Comput. Mater. Sci.*, 2014, **95**, 592.
37 J. Wang, S. Yip, S. R. Phillpot and D. Wolf, Crystal instabilities at finite strain, *Phys. Rev. Lett.*, 1993, **71**, 4182.
38 L. E. Bell, Cooling, heating, generating power, and recovering waste heat with thermoelectric systems, *Science*, 2008, **321**, 1457.
39 I. Petsagkourakis, K. Tybrandt, X. Crispin, I. Ohkubo, N. Satoh and T. Mori, Thermoelectric materials and applications for energy harvesting power generation, *Sci. Technol. Adv. Mater.*, 2018, **19**, 836–862.
40 N. Nandihalli, C. J. Liu and T. Mori, Polymer based thermoelectric nanocomposite materials and devices: Fabrication and characteristics, *Nano Energy*, 2020, **78**, 105186.
41 B. Cai, H. L. Zhuang, J. Pei, B. Su, J. W. Li, H. Hu, Y. Jiang and J. F. Li, Spark plasma sintered Bi-Sb-Te alloys derived from ingot scrap: Maximizing thermoelectric performance by tailoring their composition and optimizing sintering time, *Nano Energy*, 2021, **85**, 106040.
42 Z. Liu, N. Sato, W. Gao, K. Yubuta, N. Kawamoto, M. Mitome, K. Kurashima, Y. Owada, K. Nagase, C. Ho Lee, J. Yi, K. Tsuchiya and T. Mori, Demonstration of ultrahigh thermoelectric efficiency of ~7.3% in Mg_3Sb_2/MgAgSb module for low-temperature energy harvesting, *Joule*, 2021, **5**, 1196.
43 R. Ang, A. U. Khan, N. Tsujii, K. Takai, R. Nakamura and T. Mori, Thermoelectricity Generation and Electron-Magnon Scattering in a Natural Chalcopyrite Mineral from a Deep-Sea Hydrothermal Vent, *Angew. Chem., Int. Ed.*, 2015, **54**, 12909.
44 F. Ahmed, N. Tsujii and T. Mori, Thermoelectric properties of $CuGa_{1-x}Mn_xTe_2$: power factor enhancement by

incorporation of magnetic ions, *J. Mater. Chem. A*, 2017, **5**, 7545.

45 Y. Zheng, T. Lu, M. M. H. Polash, M. Rasoulianboroujeni, N. Liu, M. E. Manley, Y. Deng, P. J. Sun, X. L. Chen, R. P. Hermann, D. Vashaee, J. P. Heremans and H. Zhao, Paramagnon drag in high thermoelectric figure of merit Li-doped MnTe, *Sci. Adv.*, 2019, **5**, eaat9461, DOI: **10.1126/sciadv.aat9461**.

46 J. B. Vaney, S. A. Yamini, H. Takaki, K. Kobayashi, N. Kobayashi and T. Mori, Magnetism-mediated thermoelectric performance of the Cr-doped bismuth telluride tetradymite, *Mater. Today Phys.*, 2019, **9**, 100090.

47 B. He, C. Sahin, S. R. Boona, B. C. Sales, Y. Pan, C. Felser, M. E. Flatte and J. P. Heremans, Large magnon-induced anomalous Nernst conductivity in single-crystal MnBi, *Joule*, 2021, **5**, 3057.

48 R. Ullah, M. A. Ali, G. Murtaza, A. Mahmood and S. M. Ramay, The significance of anti-fluorite Cs_2NbI_6 *via* its structural, electronic, magnetic, optical and thermoelectric properties, *Int. J. Energy Res.*, 2020, **44**, 10179.

49 M. Ullah, S. A. Khan, G. Murtaza, R. Khenata, N. Ullah and S. B. Omran, Electronic, thermoelectric and magnetic properties of La_2NiMnO_6 and La_2CoMnO_6, *J. Magn. Magn. Mater.*, 2015, **377**, 197.

50 O. Rabin, Y. M. Lin and M. S. Dresselhaus, Anomalously high thermoelectric figure of merit in $Bi_{1-x}Sb_xBi_{1-x}Sb_x$ nanowires by carrier pocket alignment, *Appl. Phys. Lett.*, 2001, **79**, 81.

51 R. Ullah, M. Ali, G. Murtaza, A. Mahmmod and S. M. Ramay, An investigation of structural, elastic, mechanical, electronic, magnetic and thermoelectric properties of ferromagnetic half metallic $EuCrO_3$, *Mater. Sci. Semicond. Process.*, 2020, **122**, 105487.

52 A. U. Haq, G. M. Mustafa, M. Amin, S. M. Ramay and A. Mahmood, Ab-initio study of opto-electronic and thermoelectric properties of direct bandgap double perovskites Rb_2XGaBr_6 (X=Na, K), *Int. J. Energy Res.*, 2021, **45**, 9241.

53 S. Iqbal, G. M. Mustafa, M. Asghar, N. A. Noor, M. W. Iqbal, A. Mahmood and Y.-H. Shin, Tuning the optoelectronic and thermoelectric characteristics of narrow bandgap Rb2AlInX6(X= Cl, Br, I) double perovskites: A DFT study, *Mater. Sci. Semicond. Process*, 2022, **143**, 106551.

54 P. A. Nawaz, G. M. Mustafa, S. Sagar, N. A. Noor, T. S. Ahmad, A. Mahmood and R. Neffati, Theoretical investigations of optoelectronic and transport properties of Rb2YInX6 (X = Cl, Br, I) double perovskite materials for solar cell applications, *Sol. Energy*, 2022, **231**, 586.

55 G. A. Slack, Nonmetallic crystals with high thermal conductivity, *J. Phys. Chem. Solids*, 1973, **34**, 321.

56 M. Jamal, S. J. Asadabadi, I. Ahmad and H. A. R. Aliabad, Elastic constants of cubic crystals, *Comput. Mater. Sci.*, 2014, **95**, 592.